Gradient Artefact Modelling Using a Set of Sinosoidal Waveforms for EEG Correction During Continuous fMRI

José L. Ferreira[*1], Pierre J.M. Cluitmans[2], Ronald M. Aarts[3]

[1,2,3]Department of Electrical Engineering, Eindhoven University of Technology

[2]Kempenhaeghe Epilepsy Center

[3]Philips Research Laboratories Eindhoven
P. O. 513 5600 MB Eindhoven Netherlands

[*1]j.l.ferreira@tue.nl; [2]p.j.m.cluitmans@tue.nl; [3]r.m.aarts@tue.nl

Abstract

Simultaneous use of EEG and fMRI has become a powerful and attractive multimodal brain imaging technique in recent years, and has been broadly employed in neuroscience research as well as in clinical practice. The possibility to integrate the high temporal resolution of EEG with the high spatial resolution of fMRI constitutes one of the relevant advantages of using combined EEG-fMRI. Meanwhile, a number of challenges have to be overcome in order to consolidate such a technique as an independent and effective method to brain imaging. In particular, the artefacts which arise in the EEG signal, induced by varying gradient magnetic fields within the fMRI magnetic scanner. This work presents a novel methodology for waveform artefact modelling in order to subtract and clean up the EEG recordings. Implementation of our method results from the combination of two techniques: a non-linear low-pass filter approach based upon the slope adaption between consecutive samples of the signal (SSD); and the modelling proposal for the underlying gradient artefact components which is implemented using the sum of a set of sinusoid waveforms. The resulting EEG restoration obtained by our methodology shows to be similar to the artefact correction achieved by the established average artefact subtraction (AAS) method. Moreover, the proposed mathematical model for the artefact components shows to predict the variability of the artefact waveform over the time.

Keywords

Combined EEG-fMRI; Gradient Artefact Removal; Artefact Modelling; Signal Slope Adaption

Introduction

Acquisition of the electroencephalogram during functional magnetic resonance imaging (combined EEG-fMRI) is a multimodal technique for brain activity mapping which has achieved a wide usage in research and clinical purposes due to its powerful capability to provide new insights into the brain function (Villringer et al., 2010). The advent of the functional magnetic resonance imaging (fMRI) around two decades ago (Belliveau et al., 1991) allowed the combination of this method with electroencephalography (EEG) in studies of epilepsy (Warach et al., 1996; Seeck et al., 1998). Combined EEG-fMRI revealed itself not to be only an additional monitoring tool, but a promising technique for brain activity mapping. Nowadays, it has been extended to other types of neuroscientific studies and attracted the interest of several researchers and clinicians (Ritter and Villringer, 2006).

According to Villringer et al. (2010), as being complementary methods, only simultaneous EEG-fMRI offers the opportunity to relate brain imaging modalities to actual brain events, because the high temporal and spatial measurements which are achieved by the combination of both techniques. This property may help to understand numerous questions in basic and cognitive neuroscience. In this way, combined EEG-fMRI have been used to investigate cognitive measures of memory performance, learning capabilities, location of epileptic foci, and characterization of the relationship between epileptic electric activity and hemodynamic response (Villringer et al., 2010; Ritter and Villringer, 2006).

Parallel to the breakthroughs achieved by using simultaneous EEG-fMRI, technical problems associated with the induction of spurious voltages in the EEG in the magnetic fields of the fMRI scanner are urgent to be solved in order to consolidate and

broaden its applications range. That is the case of (a) artefacts caused by the subject movement within the scanner; (b) the "ballistogram" artefact, induced in the EEG electrodes by the pulsatile movement of the blood in scalp arteries within the static magnetic field of the fMRI equipment (B_0) (Allen et al., 1998); and (c) the "gradient" or "imaging acquisition" artefact, caused by the variation of the gradient magnetic fields within the fMRI scanner (Allen et al., 2000; Mulert and Hegerl, 2009; Ritter et al., 2010).

According to Ritter et al. (2010), gradient artefacts occur in the EEG signal due to the voltage induced by the application of rapidly varying gradient magnetic fields for spatial encoding of the magnetic resonance signal (MR), and radiofrequency pulses (RF) for spin excitation in the circuit formed by the electrodes, leads, patient and amplifier. The waveform of the gradient artefact caused by one gradient pulse is approximately the differential waveform of the corresponding gradient pulse (Anami et al., 2003; Ritter et al., 2010). Imaging acquisition artefacts have amplitudes that can be several orders of magnitude higher than that of the neuronal EEG signal. Artefact amplitudes associated with the gradient switching (10^3 to 10^4 μV) are generally much larger than those arising from RF pulses (up to 10^2 μV) (Ritter et al., 2010). As discussed by these authors, gradient artefacts have a strong deterministic component because of the pre-programmed nature of RF and gradient switching sequence (EPI sequence). In addition to exceeding the bandwidth of the standard clinical EEG, the gradient artefact frequencies overlap the EEG frequency band in discrete harmonic frequency intervals or "frequency bins", whose fundamental corresponds to the inverse of the EPI slice time parameter (Niazy et al., 2005).

In the literature, various techniques have been suggested in order to minimize the effects of the gradient artefacts in the EEG signal. For example, it is possible to reduce their magnitude at the source by laying out and immobilizing the EEG leads, twisting leads, using a bipolar electrode configuration, and using a head vacuum cushion. Furthermore, depending on the application, a periodic interleaved approach, whereby the MR signal acquisition is suspended at regular intervals, could be used as well (Ritter et al., 2010). Mullinger et al. (2011) also proposed a procedure for reduction of the magnitude of gradient artefacts by adjusting the subject position within the fMRI scanner. Regarding continuous MR acquisition, dedicated software solutions have to be developed for gradient artefacts removal in the electroencephalogram (Gonçalves et al., 2007). Thus, post-processing signal methods like frequency-domain filtering (Hoffmann et al., 2000; Sijbers et al., 1999; Sijbers et al., 2000), average artefact subtraction (AAS) (Allen et al. 2000), principal component analysis (Negishi et al., 2004; Niazy et al., 2005), independent component analysis (Mantini et al., 2007), and spatial filtering (Brookes et al., 2007) have been proposed and employed for artefact correction.

Amongst these techniques, the average artefact subtraction (AAS) methodology, the most popular for imaging artefact correction, consists of the calculation of an average artefact waveform or template over a fixed number of samples, which is then subtracted from the EEG signal at each sample (Allen et al., 2000). However, although the AAS allows a substantial removal of the gradient artefact, it is assumed that the arterfact template has a constant morphology over the time and, therefore, the variability of the artefact waveform is excluded from consideration. Thereby, after the subtraction is performed, artefact residuals arise in the signal and further processing methods must be carried out in order to achieve a satisfactory signal correction. Moreover, effectiveness of the AAS depends on accurate sampling of the gradient artefact waveform and timing-alignment of the MR scanner and EEG clocks (Mandelkow et al., 2006; Gonçalves et al., 2007; Freyer et al., 2009). Bénar et al. (2003) also indicated that average subtraction processing often leaves some remaining artefact inside the signal frames.

The current work presents a novel methodology for modelling the gradient artefact waveform to be subtracted and restore the EEG signal. Our method combines two correction approaches: application of a non-linear low-pass filter followed by estimation and subtraction of the proposed artefact waveform model per se. The non-linear low-pass filter approach, modified from Ferreira et al. (2012), makes use of the information of high-frequency activity contained in the difference between consecutive samples of the digital signal. In addition to filter high-frequency components, this approach allows higher attenuation of low-frequency artefact components as well as less distortion in the signal. In turn, the sum of a set of sinusoidal waveforms constitutes the basis of the proposed artefact waveform model. Our methodology

shows to perform effective artefact removal and EEG restoration, whose results are very similar to those obtained by AAS method. Furthermore, the proposed gradient artefact modelling approach shows to predict the variability of the artefact waveform over the time, which fails to be achieved by the artefact waveform averaging. Extensive EPI parameter calculation, data segmentation and time alignment are not required as well, as shown in the Section Materials and Methods.

Materials and Methods

Patients

Simultaneous EEG and fMRI data have been collected for a research focused on epilepsy and post-traumatic stress disorder (PTSD) (Van Liempt et al., 2011), jointly developed by the department of Psychiatry of Universiteit Medisch Centrum Utrecht, the Research Centre Military Mental Health Care in the Dutch Central Military Hospital in Utrecht, and the Department of Research and Development of the Kempenhaeghe Epilepsy Center in Heeze, The Netherlands.

Data were recorded from military veterans with PTSD which were in mission abroad through the outpatient clinic of the Military Mental Health Care. All participants were male at the age between 18 and 60 years. EEG signal recordings from 15 subjects were used in order to apply and evaluate the methodology we have proposed in this work.

Protocol for Data Acquisition

Functional magnetic resonance imaging scanning was carried out using a 3 T Scanner (Philips, Eindhoven, and The Netherlands) at Kempenhaeghe Epilepsy Center. An MRI-compatible 64 channel polysomnograph was used to collect one ECG channel, two EOG channels, one EMG and 60 EEG channels. The EEG electrodes positioning was in accordance with the 10 – 20 international system electrodes placement. The sampling frequency for EEG signal acquisition was 2048 Hz.

Combined EEG-fMRI data were collected during 45 minutes, after application of the EEG cap. The subjects were scanned using a functional echo-planar imaging sequence with 33 transversal slices (thickness 3 mm, TE 30 ms, and TR 2500 ms).

Block Diagram of the Proposed Methodology

Implementation of our methodology for waveform artefact modelling and EEG restoration was divided into four steps, according to the algorithm structure block diagram of Fig. 1:

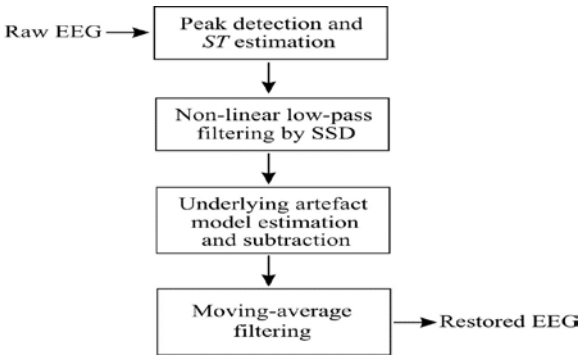

FIG. 1 PROPOSED ALGORITHM STRUCTURE FOR GRADIENT ARTEFACT MODELLING AND EEG RESTORATION

Each step was developed and applied to the EEG recordings in MATLAB environment.

Peak Identification for ST Estimation

Estimation of the EPI parameter slice time (*ST*) was performed for determination of the EEG window length to be processed as well as the fundamental frequencies of the frequency bins (Niazy et al., 2005). Observation of the raw data recorded within the MR scanning revealed the occurrence of the steep wave activity or typical peaks corresponding to the onset of each MR slice. Thereby, *ST* could be estimated by evaluation of the time interval between two subsequent peaks (Garreffa et al., 2003).

In order to detect the peaks, initially, a signal threshold has been estimated according to the peak detection algorithms proposed by Garreffa et al. (2003). Considering the data under analysis, the value of *ST* was estimated at 155 ± 1 samples, which corresponded to the time interval of 75.68 ± 0.50 ms (Ferreira et al., 2012).

The EEG window length was set as a multiple of *ST*. This is a required condition during estimation of the underlying gradient artefact components within the EEG bandwidth, as described below. Hence, an EEG window of 32 slices was employed, i.e., 32 × 155 samples.

Non-linear Low-pass Filtering Using Signal Slope Adaption (SSD)

To remove high-frequency artefact components, a non-linear low-pass filter was developed and utilized based upon the difference of consecutive samples of the digital signal, the signal slope adaption – SSD (Ferreira et al., 2013). Such a filter was implemented by

taking into account the idea of estimating the variability of the residuals resulting from application of the AAS method, as described in Ferreira et al. (2012). We would rather use such a filter because, in addition to being a zero-phase filter, it provokes less distortion in the frames of the filtered signal as well causes higher attenuation of the underlying artefact components in the EEG bandwidth. These features leaded to the minimization of the occurrence of artefact residuals in the restored EEG.

The analysis of the signal slope represented by the difference between consecutive samples can be employed to detecting high-frequency properties and artefacts in digital signals (Scherg, 1982; Barlow, 1983; Cluitmans et al., 1993; Van de Velde et al., 1998; Ferreira et al., 2012). Cluitmans et al. (1993) and Van de Velde et al. (1998) proposed a methodology which makes use of such a signal parameter, associated with large signal magnitudes, for detection of the high-frequency activity related to the muscle artefact in the EEG signal. In the same way, observation of the EEG recorded within the fMRI scanner reveals that large slopes and magnitudes of the signal can be attributed to the gradient artefact and its residuals as well (Koskinen and Vartiainen, 2009; Ferreira et al., 2012).

According to Ferreira et al. (2012), the larger slopes related to the sharp wave activity of the gradient artefact residuals are used to identify whether the EEG samples are artefact free or not. In order to perform the identification, a slope threshold (*thrs*) is estimated in such a way that if the sample has signal slope larger than *thrs*, it is then identified as containing artefact interference. *thrs* can be estimated, for example, taking into account the probability distribution of the signal slope (Cluitmans et al., 1993; Van de Velde et al., 1998). As discussed by Ferreira et al. (2012), it is possible to approximate the raw EEG (**EEG**$_{\mathbf{raw}}$) to the true EEG (**EEG**$_{\mathbf{true}}$), using the approach proposed by Klados et al. (2009). According to this approach, as the value of a filter parameter $\hat{a}_i$ is approximated to the optimal parameter value a_i, the values of the **EEG**$_{\mathbf{raw}}$ would tend to the true EEG:

$$\lim_{\hat{a}_i \to a_i} EEG_{raw,i} = EEG_{true,i}. \tag{1}$$

Here, the difference between consecutive samples of the signal, *diff* (**EEG**$_{\mathbf{raw}}$), has been assumed as the filter parameter $\hat{a}_i$, and the slope threshold *thrs* as the optimal value a_i. Taking into account a window whose number of points is equal to the length of the raw EEG, the maximum absolute value of the difference between consecutive samples of the signal **EEG**$_{\mathbf{raw}}$ corresponds to the parameter r_i which is related to *diff* (**EEG**$_{\mathbf{raw}}$) by the following expression (Ferreira et al., 2013):

$$r_i = \max \left| diff(\mathbf{EEG}_{\mathbf{raw}}) \right|, \tag{2}$$

where i is the subscript of the maximum slope within *diff* **(EEG**$_{\mathbf{raw}}$**)**.

The two consecutive samples $EEG_{raw,i}$ and $EEG_{raw,i+1}$ associated with r_i are adapted as follows:

$$\begin{aligned} EEG_{corct,i} &= EEG_{raw,i} - L_i, \\ EEG_{corct,i+1} &= EEG_{raw,i+1} + L_i, \end{aligned} \tag{3}$$

where

$$L_i = p \times r_i. \tag{4}$$

p corresponds to the adaption factor $(0 < p < 1)$ to be applied to the parameter r_i. An appropriate value of p was experimentally determined and set to be 0.925. In (3), the sign of L_i is set positive when $EEG_{raw,i} > EEG_{raw,i+1}$, and vice-versa. The signal **EEG**$_{\mathbf{raw}}$ in equation (3) is then replaced by the modified signal **EEG**$_{\mathbf{corct}}$, which contains the adapted samples $EEG_{corct,i}$ and $EEG_{corct,i+1}$. (2), (3) and (4) are iteratively recalculated until $r_i \le thrs$. The decreasing value of r_i calculated at each iteration ensures the convergence of (3).

Estimation of *thrs* has been performed by taking into account probability distributions of an artefact free EEG interval (**EEG**$_{\mathbf{true}}$) and an EEG excerpt containing artefacts, both of which picked up from the same EEG channel. The true EEG was obtained from the raw EEG recorded within the scanner without gradient magnetic field variation. It has been observed from the probability distributions that more than around 95% of the values for the signal slope of the raw EEG, *diff* (**EEG**$_{\mathbf{raw}}$), lay outside the range $\mu_{diff(\mathbf{EEG}_{\mathbf{true}})} + 3\sigma_{diff(\mathbf{EEG}_{\mathbf{true}})}$ estimated for the signal slope of artefact free EEG segments. Further, the probability distribution of the slope parameter estimated for the true EEG closely resembles Gaussian distributions (Cluitmans et al., 1993), in such a way that the confidence interval associated with $\mu_{diff(\mathbf{EEG}_{\mathbf{true}})} + 3\sigma_{diff(\mathbf{EEG}_{\mathbf{true}})}$ encompasses approximately 99.5% of the distribution (Papoulis and Pillai, 2002). Thereby, estimation of *thrs* was performed by Eq. (5):

$$thrs = \mu_{diff(\mathbf{EEG}_{\mathbf{true}})} + 3\sigma_{diff(\mathbf{EEG}_{\mathbf{true}})}. \tag{5}$$

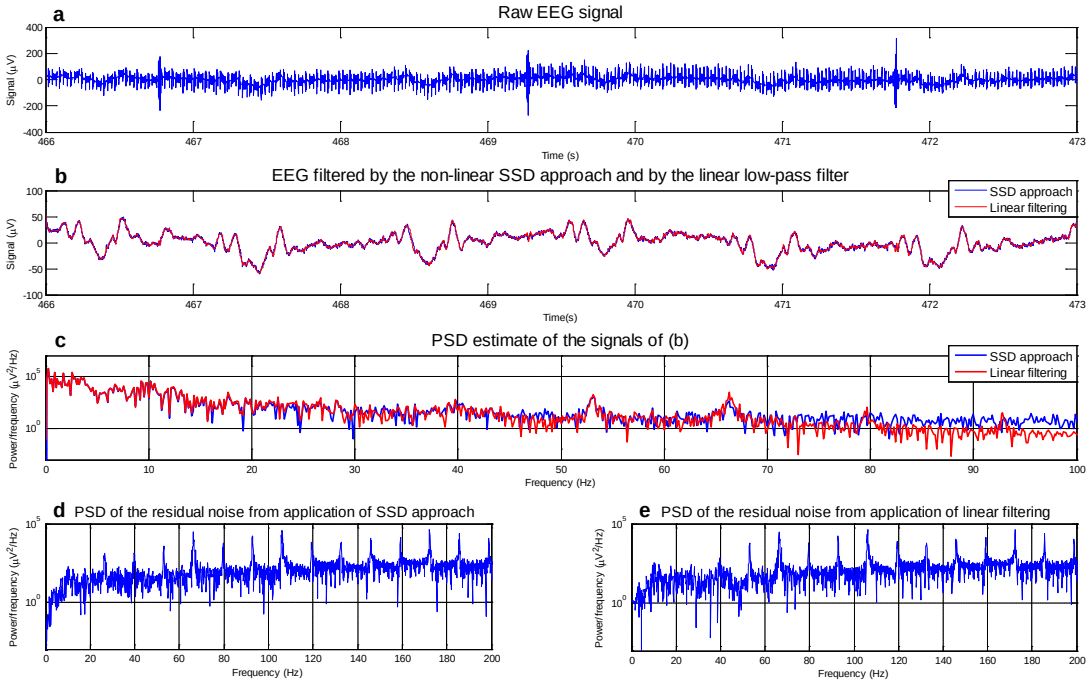

FIG. 2 COMPARISON BETWEEN THE APPLICATION OF THE SSD NON-LINEAR LOW-PASS FILTER AND A LINEAR LOW-PASS FILTER

Fig. 2 illustrates how the SSD approach filters the high-frequency artefact components. Fig. 2b depicts the resulting signals from application of the SSD approach and a linear low-pass filter, FIR, 55-coefficients, cut-off frequency of 70 Hz, to the raw EEG segment of Fig. 2a. This EEG excerpt was selected from the recordings of one specific patient, electrode position P3. The standard deviation of the subtraction between the corrected signals of Fig. 2b is estimated at 2.1 μV. In Fig. 2c, the PSD estimates of the signals of Fig. 2b are depicted. In turn, Figs. 2d and 2e depict the residual noise associated with application of both filtering approaches. This figure evidences that the SSD filter provokes higher attenuation of low-frequency artefact components. Frequency components corresponding to the harmonics of the repetitive slice sequence (multiples of 13.2 Hz) are well attenuated in the bandwidth under the filter cut-off frequency (Fig. 2d), whereas PSD estimate of Fig. 2e shows higher attenuation of such components around 70 Hz.

Modelling and Subtraction of Underlying Artefact Components

As underlying artefact components remain in the **EEG**$_{corct}$ bandwidth after application of the low-pass filter described by Eqs. (2) – (5), elimination of such components is still necessary in order to restore the EEG signal (Allen et al., 2000; Niazy et al., 2005). In this respect, the following model was proposed to describe the components of the signal **EEG**$_{corct}$:

$$EEG_{corct,i} = \hat{EEG}_{true,i} + \sum_{k=1}^{K} har_{k,i} + n_i \quad (6)$$

where $\hat{EEG}_{true,i}$ is the estimate of the true EEG cleaned from gradient artefacts; har_k corresponds to the fundamental of the *k-th* artefact harmonic component to be removed amongst the total of K harmonic components taken into account ($K = 7$); and n_i corresponds to the additional noise. Frequency components above $K = 7$ have been neglected since they are removed by the SSD low-pass filter.

The proposed mathematical model for the artefact components har_k was based upon the analysis of the shape and amplitude of average artefact templates obtained from application of the AAS method (Allen et al., 2000) to the signal **EEG**$_{corct}$. It has been proposed that each artefact harmonic component can be approximated by a sinusoidal waveform described as:

$$har_k = A_k \cos(2\pi f_k t + \theta_k), \quad (7)$$

where

$$A_k = \frac{2 \times |S_{corct,k}|}{N}, \quad (8)$$

and $S_{corct,k}$ is the spectral amplitude (FFT) of the *k-th* gradient artefact harmonic component within the **EEG**$_{corct}$. N corresponds to the length of the **EEG**$_{corct}$,

which must be a multiple of the slice time, *ST*. This requirement allows estimating the value of A_k corresponding to the frequency f_k which, in turn, is provided by Eq. (9):

$$f_k = k\frac{f_s}{ST}, \qquad (9)$$

where f_s is the EEG sampling rate. Finally, the phase of (7) is calculated by.

$$\theta_k = m_k \times \pi, \qquad (10)$$

where m_k is a number between 0 and 2, estimated in such a way that the subtraction of har_k from the $\mathbf{EEG}_{corct}$ minimizes the value of the spectral amplitude of the *k-th* gradient harmonic artefact component in the resulting EEG signal.

The modelling of the adjacent frequency components to the *k-th* harmonic has been taken into account, which occurs in the frequency bins as well**.** These frequency components arise into the region of ±1 Hz around the *k-th* harmonic (Niazy et al., 2005). Thereby, the immediate upper and lower frequency components inside the bins were inserted into the artefact waveform model and subtracted from the $\mathbf{EEG}_{corct}$**.**

After subtraction of the underlying artefact components from the $\mathbf{EEG}_{corct}$, a 14-point moving-average (MA) filter (Fig. 1) was employed to smooth and, thus, additional correction associated with n_i in (6) has been achieved. Hence, the resulting restored EEG corresponds to the signal $\mathbf{E\hat{E}G}_{true}$**.**

Validation

Our proposed methodology was applied in raw EEG excerpts collected from a set of validation EEG channels: FP1, F3, F8, T5, P3, Oz, CP1, FC5, AFz, F6, C2, TP7, CP4, and POz. The artefact waveform model and the EEG restoration achieved by our methodology were compared to those obtained by the AAS method (Allen et al., 2000). In addition, the reduction of the average spectral power associated to the artefact frequency bins was assessed, as performed by Niazy et al. (2005).

Results

Application of our methodology is illustrated in Fig. 3. Fig. 3b shows a representative signal $\mathbf{EEG}_{corct}$ resulting from the application of the non-linear low-pass filter in a raw EEG excerpt which contains strong artefact interference (Fig. 3a). This EEG excerpt was selected from the recordings of one subject, electrode position F8. In order to model and remove the underlying artefact components within the EEG bandwidth, Eqs. (6) – (10) were then applied to the $\mathbf{EEG}_{corct}$, resulting in the signal depicted in Fig. 3c. The restored EEG signal, after application of the MA filter in the signal of Fig. 3c, is shown in Fig. 3d.

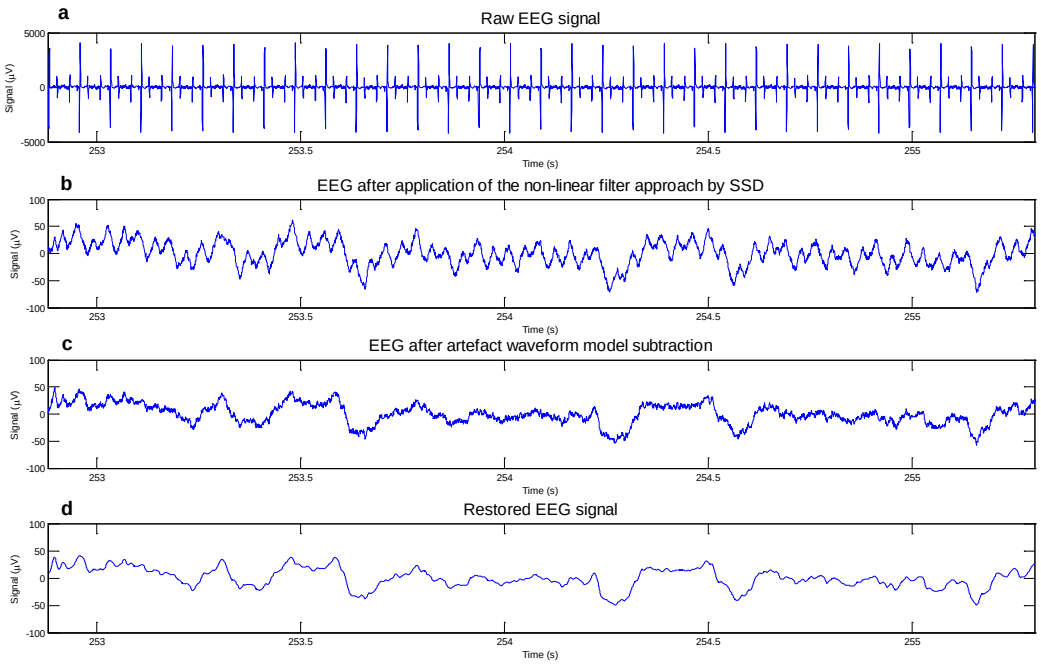

FIG. 3 APPLICATION OF OUR METHODOLOGY TO (A) A RAW EEG SIGNAL WITH STRONG GRADIENT ARTEFACT INTERFERENCE; (B) $\mathbf{EEG}_{CORT}$, RESULTING FROM APPLICATION OF THE NON-LINEAR LOW-PASS FILTER USING THE SSD APPROACH; (C) EEG SIGNAL AFTER SUBTRACTION OF OUR PROPOSED ARTEFACT MODEL; (D) RESTORED EEG SIGNAL

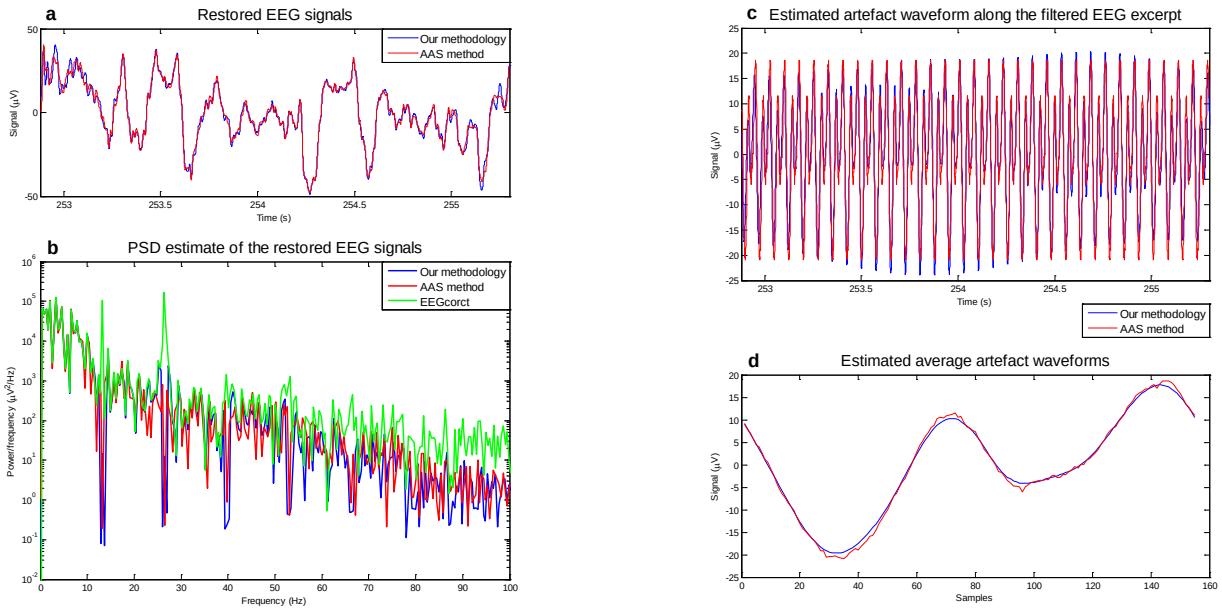

FIG. 4 COMPARISON BETWEEN THE RESULTS OBTAINED BY OUR METHODOLOGY AND THE AAS METHOD: (A) RESTORED EEG SIGNALS (B) PSD ESTIMATE OF THE RESTORED SIGNALS; (C) ARTEFACT WAVEFORMS FOR THE ENTIRE EEG EXCERPT; (D) AVERAGE ARTEFACT WAVEFORMS (155 SAMPLES)

Fig. 4 depicts a comparison between the signal restorations obtained from the application of our methodology and the AAS method in the $\mathbf{EEG}_{\mathbf{corct}}$ of Fig. 3b. A strong proximity between the restored EEG signals can be observed (Figs. 4a and 4b), which was confirmed by the median of the standard deviation of the difference between the restored signals by both methodologies (at 2.3 μV), and the median of the estimated averaged artefact waveforms (at 0.6 μV), considering the set of EEG validation channels. However, unlike an artefact template, the artefact waveform modelled by Eqs. (6) – (10) is estimated over the EEG excerpt. As noticed in Fig. 4c, such a model shows variability over the time. The averaged waveform (blue trace) shown in Fig. 4d did result from averaging of our proposed model depicted in Fig. 4c, segmented and interpolated according to the slice-timing in the raw EEG signal (as performed by the AAS methodology).

Yet, it has been observed that as the length of the EEG excerpt is increased, the standard deviation of the difference between the artefact waveforms of Fig. 4c tends to decrease and, therefore, such models are approximated. According to the artefact correction achieved by our methodology, the median value of the imaging artefact (Allen et al., 2000) calculated considering the validation EEG channels was 2.6 μV pk-pk (prior to the application of the MA filter).

Fig. 5 shows the power spectrum of the artefact waveform estimated by our methodology, depicted in Fig. 4c, in which the peaks correspond to the spectral power attenuated within the artefact frequency bins.

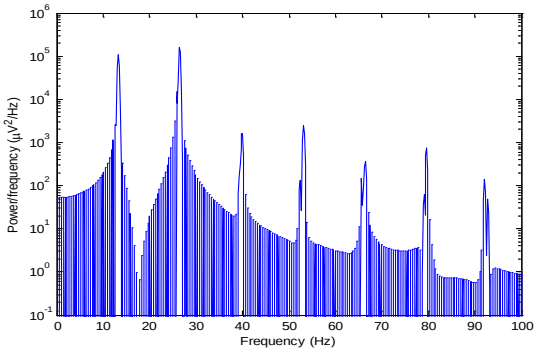

FIG. 5 POWER SPECTRUM OF THE ARTEFACT MODEL ESTIMATED BY OUR METHODOLOGY, DEPICTED IN FIG. 4C

Considering the EEG validation channels, the median spectral power attenuation within the frequency bins 13.2, 26.4, 39.6, 52.9, 66.1, 79.3, and 92.5 Hz achieved by the application of the non-linear low-pass filter was respectively, 71.4%, 94.5%, 99.8%, 99.8%, 99.9%, 99.9%, and 99.9%. Concerning the frequency bands 0 – 4 Hz, 4 – 8 Hz, 8 –12 Hz, and 12 – 24 Hz, the respective median spectral power reduction after the subtraction of the proposed artefact waveform model was 0.3%,

0.6%, 2.3%, and 68%. The higher attenuation in the range 12 – 24 Hz corresponds to the region in which the occurrence of removal of components is associated with the frequency bins 13.2 and 26.4 Hz.

Discussion

Although the artefact resulting from the gradient magnetic fields switching has a strong deterministic component (Ritter et al., 2010), it is also affected by other sources of interference like scanner vibration, subject movements during the studies as well as inaccurate slice alignment between EEG and fMRI clocks. Because of this, the morphology of the artefact waveform is not constant over the time (Gonçalves et al., 2007; Sun and Hinrichs, 2009). Thus, investigation of a more accurate artefact template during the EEG restoration by the AAS method (Allen et al., 2000) has been often reported in the literature (Mandelkow et al., 2006; Gonçalves et al., 2007; Moosmann et al., 2009; Koskinen and Vartiainen, 2009).

The imaging artefact waveform is approximately the differential waveform of the MR and RF gradient magnetic fields (Brown and Semelka, 2003; Anami et al., 2003; Ritter et al., 2010) which are constituted by sinusoidal components as well. Thereby, modelling of the artefact as sinusoids appears to be a reasonable approach. This idea is confirmed by the analysis of the artefact template estimated by the AAS method after application of the non-linear low-pass filter described by Eqs. (2) – (5).

Hence, the model described by Eqs. (6) – (10) has been put forward which performs estimation of the artefact waveform by the sum of a set of sinusoidal waveform components. According to our approach, the artefacts components contained into the frequency bins regions (Niazy et al., 2005) are modelled as sinusoids in the time-domain (Eq. 7), whereas the respective sinusoidal parameters are estimated in the frequency-domain (Eqs. (8), (9), and (10)). As observed in Fig. 4e, the averaged artefact waveform obtained from our methodology is quite similar to that estimated by application of the AAS method. In the same way, the overall EEG restoration achieved by both methodologies is very similar (Fig. 4). Clearly, it confirms the hypothesis described by the modelling proposal of Eqs. (6) – (10). On the other hand, the model calculated by our methodology shows to predict the variability of the artefact waveform morphology over the time (Fig. 4c), which is not observed for the artefact template obtained from the AAS method. The use of an analytical model instead an average template could explain this characteristic observed within our modelling approach.

It is also noticed that as the window of the processed EEG is increased, the model estimated by our methodology approximates to the model estimated by the AAS method. This fact suggests that, as our proposed model is constituted by the average of sinusoids estimated over the EEG interval, it would tend to approach to the average model obtained from the AAS method for larger EEG excerpts. Furthermore, concerning application of the methodology depicted in Fig. 1 in EEG excerpts of the other channels, it is revealed that the estimated waveform model showed a variation from channel to channel, as expected.

The usage of the non-linear filter described by Eqs. (2) – (5) reveals the achievement of a better attenuation of the spectral power associated with the low-frequency artefact components (Fig. 2) as well as less distortion of in the signal frames. These characteristics allowed minimizing the occurrence of artefact residuals in the restored EEG. Improvements of the computational performance of such a filter shall be done in future work. Likewise, our methodology should be assessed for other types of fMRI scanners. As another suggestion for future work, the possibility to combine our method with the AAS methodology and other artefact correction techniques should be investigated as well.

Conclusions

In this work, a mathematical model based upon the sum of a set of sinusoidal waveforms is proposed for gradient artefact correction during continuous EEG-fMRI. Estimation and model subtraction for restoration of the EEG signal are performed after application of a non-linear filter, which makes use of the high-frequency information contained in the larger artefact signal slopes.

In addition to the operation of an EEG restoration quite similar to that obtained from the AAS method, our methodology predicts the artefact waveform variability over the time, instead a template with constant morphology.

Such characteristics could enable the usage of our method on seeking a more precise artefact waveform. Thereby, its combination with AAS itself and other correction approaches could improve the quality of the restored EEG signal and, thereby, enlarging the range of applications of the combined EEG-fMRI technique.

ACKNOWLEDGMENT

We are grateful to Saskia van Liempt, M.D., and Col. Eric Vermetten, M.D., Ph.D. from the University Medical Center/Central Military Hospital, Utrecht, for providing the data presented in this work. This work has been made possible by a grant from the European Union and Erasmus Mundus – EBW II Project, and by a grant from CNPq – Science without Borders Program.

REFERENCES

Allen, P., Polizzi, G., Krakow, K., Fish, D., Lemieux, L. "Identification of EEG Events in the MR Scanner: the Problem of Pulse Artefact and a Method for Its Subtraction." Neuroimage 8 (1998): 229-239.

Allen, P., Josephs, O., Turner, R. "A Method for Removing Imaging Artifact from Continuous EEG Recorded during Functional MRI." NeuroImage 12 (2000): 230-239.

Anami, K. et al. "Stepping Stone Sampling for Retrieving Artifact-Free Electroencephalogram during Functional Magnetic Resonance Imaging." NeuroImage 19 (2003): 281–295.

Barlow, J. "Muscle Spike Artifact Minimization in EEGs by Time-Domain Filtering." Electroencephalogr. Clin. Neurophysiol. 55 (1983): 487–491.

Belliveau, J. et al. "Functional Mapping of the Human Visual-Cortex by Magnetic Resonance-Imaging." Science 254 (1991): 716–719.

Bénar, C. et al. "Quality of EEG in Simultaneous EEG-fMRI for Epilepsy." Clin. Neurophysiol. 114 (2003): 569-580.

Brookes, M., Mullinger, K., Stevenson, C., Morris, P., Bowtell, R. "Simultaneous EEG Source Localisation and Artefact Rejection during Concurrent fMRI by Means of Spatial Filtering." NeuroImage 40 (2008): 1090-1104.

Brown, M., Semelka, R. MRI: Basic Principles and Applications. 4th Ed. New York: Wiley, 2003.

Cluitmans, P., Jansen, J., Beneken, J. "Artefact Detection and Removal during Auditory Evoked Potential Monitoring." J. Clin. Monit. 9 (1993): 112–120.

Ferreira, J., Cluitmans, P., Aarts, R.M. "Gradient Artefact Correction in the EEG Signal Recorded within the fMRI scanner." 5th International Conference on Bio-Inspired Systems and Signal Processing, BIOSIGNALS 2012, Vilamoura, Portugal, February 1-4, 2012, Proceedings: 110-117, 2012.

Ferreira, J., Cluitmans, P., Aarts, R.M. "Detection of Sharp Wave Activity in Biological Signals Using Differentiation between Consecutive Samples." 6th International Conference on Bio-Inspired Systems and Signal Processing, BIOSIGNALS 2013, Barcelona, Spain, February 11-14, 2013, Proceedings: 327-332, 2013.

Freyer, F., Becker, R., Anami, K., Curio, G., Villringer, A., Ritter, P. "Ultrahigh-Frequency EEG during fMRI: Pushing the Limits of Imaging-Artifact Correction." NeuroImage 48 (2009): 94-108.

Garreffa, G. et. al. "Real-time MR Artifacts Filtering during Continuous EEG/fMRI Acquisition." Magn. Res. Imaging. 21 (2003): 1175-1189.

Gonçalves, S., Pouwels, P., Kuijer, J., Heethaar, R., de Munck, J. "Artifact Removal in Co-Registered EEG/fMRI by Selective Average Subtraction." Clin. Neurophysiol. 118 (2007): 823-838.

Hoffmann, A., Jäger, L., Werhahn, K., Jaschke, M., Noachtar, S., Reiser, M. "Electroencephalography during Functional Echo-Planar Imaging: Detection of Epileptic Spikes Using Post-Processing Methods." Magn. Res. Med. 44 (2000): 791-798.

Klados, M., Papadelis, C., Bamidis, P. "A New Hybrid Method for EOG Artifact Rejection." 9th International Conference on Information Technology and Application in Biomedicine, ITAB 2009, Larnaca, Cyprus, November 5-7, 2009, Proceedings: 4937-4940, 2009.

Koskinen, M., Vartiainen, N. "Removal of Imaging Artifacts in EEG during Simultaneous EEG/fMRI Recording: Reconstruction of a High-Precision Artifact Template." NeuroImage. 46 (2009): 160-167.

Mandelkow, H., Halder, P., Boesiger, P., Brandeis, D. "Synchronization Facilitates Removal of MRI Artefacts from Concurrent EEG Recordings and Increases Usable bandwidth." NeuroImage 32 (2006): 1120-1126.

Mantini, D., Perucci, M., Cugini, S., Romani, G., Del Gratta, C. "Complete Artifact Removal for EEG Recorded during Continuous fMRI Using Independent Component Analysis." NeuroImage 34 (2007): 598-607.

Moosmann, M., Schönfelder, V., Specht, K., Scheeringa, R., Nordby, H., Hugdahl, K. "Realignment parameter-Informed Artefact Correction for Simultaneous EEG-

fMRI Recordings." NeuroImage 45 (2009): 1144-1150.

Mulert, C., Hegerl, U. "Integration of EEG and fMRI." In Neural Correlation of Thinking, Edited by E. Kraft, G. Gulyás, E. Pöppel, 95-106. Verlag, Berlin, Heidelberg: Springer, 2009.

Mullinger, K., Yan, W., Bowtell, R. "Reducing the Gradient Artefact in Simultaneous EEG-fMRI by Adjusting the Subject'S Axial Position." NeuroImage 54 (2011): 1942-1950.

Negishi, M., Abildgaard, M., Nixon, T., Constable, R. "Removal of Time-Varying Gradient Artifacts during Continuous fMRI." Clin. Neurophysiol. 115 (2004): 2181-92.

Niazy, R., Beckmann, C., Iannetti, G., Brady, J., Smith S. "Removal of FMRI Environment Artifacts from EEG Data Using Optimal Basis Sets." NeuroImage. 28 (2005): 720-737.

Papoulis, A.; Pillai, S. Probability, Random Variables, and Stochastic Processes. 4th ed. New York: McGraw-Hill, 2002.

Ritter, P., Becker, R., Freyer, F., Villringer, A. "EEG Quality: the Image Acquisition Artifact." In EEG-fMRI: Physiological Basis, Technique and Applications, Edited by C. Mulert, L. Limieux, 153-171. Verlag, Berlin, Heidelberg: Springer, 2010.

Ritter, P., Villringer, A. "Simultaneous EEG-fMRI." Neurosci. Biobehav. Rev. 30 (2006): 823-838.

Seeck, M. et al. "Non-Invasive Epileptic Focus Localization Using EEG-Triggered Functional MRI and Electromagnetic Tomography." Electroencephalogr. Clin. Neurophysiol. 106 (1998): 508-512.

Sijbers, J., Michiels, I., Verhoye, M., van Auderkerke, J., van der Linden, A., van Dyck, D. "Restoration of MR-Induced Artifacts in Simultaneously Recorded MR/EEG Data." Magn. Res. Imaging. 17(1999): 1383-1391.

Sijbers, J., van Audekerke, J., Verhoye, M., van der Linden, A., van Dyck, D. "Reduction of ECG and Gradient Related Artifacts in Simultaneously Recorded Human EEG/fMRI Data." Magn. Reson. Imaging. 18 (2000): 881-886.

Sun, L., Hinrichs, H. "Simultaneously Recorded EEG-fMRI: Removal of Gradient Artifacts by Subtraction of Head Movement Related Average Artifact Waveforms." Hum. Brain Mapp. 30 (2009): 3361–3377.

Van de Velde, M., Van Erp, G., Cluitmans, P. "Detection of Muscle Artefact in the Normal Human Awake EEG." Electroencephalogr. Clin. Neurophysiol. 107 (1998): 149-158.

Van Liempt, S., Vermetten, E., Arends, J., Westenberg, H. "Decreased Nocturnal Growth Hormone Secretion and Sleep Fragmentation in Combat-Related Posttraumatic Stress Disorder; Potential Predictors Of Impaired Memory Consolidation." Psychoneuroendocrino. 36 (2011): 1361-1369.

Villringer, A., Mulert, C., Lemieux, L. "Principles of Multimodal Functional Imaging and Data Integration." In EEG-fMRI: Physiological basis, technique and applications, edited by C. Mulert, L. Limieux, 3-17. Verlag, Berlin, Heidelberg: Springer, 2010.

Warach, S., Ives, J., Schlaug, G., Patel, M., Darby, D., Thangaraj, V., Edelman, R., Schomer, D. "EEG-Triggered Echo-Planar Functional MRI in epilepsy." Neurology. 47 (1996): 89-93